Published in "The European Physical Journal E 30(4): 351-359, 2009"
which should be cited to refer to this work.

Towards a structural characterization of charge-driven polymer micelles*

I.K. Voets[1,a], R. de Vries[1], R. Fokkink[1], J. Sprakel[1], R.P. May[2], A. de Keizer[1], and M.A. Cohen Stuart[1]

[1] Laboratory of Physical Chemistry and Colloid Science, Wageningen University, Dreijenplein 6, 6703 HB Wageningen, The Netherlands
[2] Institut Max von Laue-Paul Langevin, F-38042 Grenoble Cedex 9, France

Abstract. Light scattering and small-angle neutron scattering experiments were performed on comicelles of several combinations of oppositely charged (block co)polymers in aqueous solutions. Fundamental differences between the internal structure of this novel type of micelle —termed complex coacervate core micelle (C3Ms), polyion complex (PIC) micelle, block ionomer complex (BIC), or interpolyelectrolyte complex (IPEC)— and its traditional counterpart, *i.e.*, a micelle formed via self-assembly of polymeric amphiphiles, give rise to differences in scaling behaviour. Indeed, the observed dependencies of micellar size and aggregation number on corona block length, N_{corona}, are inconsistent with scaling predictions developed for polymeric micelles in the star-like and crew-cut regime. Generic C3M characteristics, such as the relatively high core solvent fraction, the low core-corona interfacial tension, and the high solubility of the coronal chains, are causing the deviations. A recently proposed scaling theory for the cross-over regime, as well as a primitive first-order self-consistent field (SCF) theory for obligatory co-assembly, follow our data more closely.

PACS. 64.75.Yz Self-assembly – 61.25.H- Macromolecular and polymers solutions; polymer melts – 82.35.Rs Polyelectrolytes

1 Introduction

Polymer self-assembly has been a topic of intense investigation for many years. Advances in polymer synthesis have provided a wide variety of copolymers differing both in composition and architecture, giving rise to various novel classes of hierarchical assemblies. One of the recent developments involves the use of electrostatic interaction between two oppositely charged blocks in aqueous solutions as a driving force for micellisation.

Nearly a century ago, the associative phase separation of two oppositely charged colloids was discovered and the term "complex coacervation" was coined by Bungenberg de Jong and Kruyt to describe the phenomenon [1]. Only much later, it was recognised that this macroscopic phase separation can be restricted to the colloidal domain, simply via attachment of a neutral, water-soluble block to one or both of the polyelectrolytes [2–4]. Instead of mixing two oppositely charged polyelectrolytes, an ionic-neutral copolymer was mixed with a polyelectrolyte or another ionic-neutral copolymer, giving rise to a novel type of micelles (fig. 1), for which several equivalent terms are in use: complex coacervate core micelles (C3Ms) [4], polyion complex (PIC) micelles [3], block ionomer complexes (BIC) [2], and interpolyelectrolyte complexes (IPEC) [5].

By now, many general physicochemical properties of C3Ms have been well established. One of the most fundamental is their tendency towards local charge compensation. The driving force for micellisation is Coulombic attraction and entropy gain through release of many small, monovalent counterions, that are replaced by a large counterion, *i.e.*, the oppositely charged polymer. The number of cationic and anionic segments within the micellar core is approximately equal, *i.e.*, C3Ms are typically formed under charge stoichiometric conditions. As the driving force is of electrostatic nature, C3Ms are inherently stimuli responsive: they react to changes in solution ionic strength and, in case of weak polyelectrolytes, *p*H. For example, addition of an excess of salt destabilises C3Ms via charge screening. Other general features, such as relatively high critical micellisation concentrations (CMC), size polydispersities, and solvent fractions, and rather low aggregation

* Supplementary material in the form of a PDF file available from the Journal web page at
http://dx.doi.org/10.1140/epje/i2009-10533-4

[a] *Present address:* Adolphe Merkle Institute, University of Fribourg, Route de l'ancienne Papeterie, CH-1723 Marly 1, Switzerland; e-mail: ilja.voets@unifr.ch

Fig. 1. Schematic representation of a complex coacervate core micelle (C3M) consisting of two diblock copolymers. The cationic (light grey) and anionic (black) polyelectrolyte blocks of the copolymers reside in the micellar core, while the neutral, water-soluble segments (dark grey) form the micellar corona.

numbers, as compared to other types of polymer micelles, are similarly related to the relatively weak nature of the driving force, *i.e.*, electrostatic interaction as opposed to hydrophobic interaction.

The scaling behaviour of structural parameters such as micellar size and aggregation number with respect to, for example, core and corona block length, is sparsely investigated [6,7]. One may anticipate similar dependencies as the ones experimentally reported and theoretically derived for micelles consisting of polymeric amphiphiles. However, it is likely that typical C3M features such as a relatively high core solvent fraction, a low core-corona interfacial tension, and a high solubility of the coronal chains, generate scaling relations that considerably deviate from those developed for hydrophobically driven self-assemblies. The present contribution describes a series of light and neutron scattering experiments that collect structural parameters of several types of C3Ms, consisting of two diblock copolymers PAA-*b*-PEO and P2MVP-*b*-PEO, of an annealed copolymer PAA-*b*-PAAm and a quenched homopolymer $P2MVP_{43}$, and of an annealed copolymer PAA-*b*-PAAm and an annealed homopolymer $PDMAEMA_{150}$, as a function of N_{PEO} and N_{PAAm}. Note that an annealed or weak copolymer contains annealed or weak polyelectrolyte segments such that it has a *p*H-dependent charge density, while a quenched or strong copolymer contains quenched or strong polyelectrolyte segments such that its charge density is *p*H-independent. The data are subsequently used to test the applicability of scaling laws derived for micelles consisting of polymeric amphiphiles to complex coacervate core micelles.

2 Materials and methods

2.1 Materials

Poly(acrylic acid)-*block*-poly(acryl amide) copolymers, PAA-*b*-PAAm, have been synthesised by RAFT with the chain transfer agent (CTA) 3-benzylsulfanyl thiocarbonylsulfanyl propionic acid, also known as benzyl propionic acid trithiocarbonate or BPATT [8]. PAAm polymerisation from a PAA_{39} and PAA_{44} precursor yielded three PAA_{39}-*b*-$PAAm_x$ copolymers ($N_{PAAm} = 97, 191, 381$) and three PAA_{44}-*b*-$PAAm_x$ ($N_{PAAm} = 150, 300, 610$) copolymers. Poly(2-vinyl pyridine)-*block*-poly(ethylene oxide) copolymers, P2VP-*b*-PEO, have been synthesised by sequential anionic polymerisation. Poly(2-vinyl pyridine), $P2VP_{43}$, polymerised via anionic polymerisation, was purchased from Polymer Standards Service (Mainz, Germany). Poly(2-(N,N-dimethylamino)ethyl methacrylate), $PDMAEMA_{150}$, poly(acrylic acid)-*block*-poly(ethylene oxide), PAA_{51}-*b*-PEO_{250}, and poly(2-vinyl pyridine)-*block*-poly(ethylene oxide), $P2MVP_{41}$-*b*-PEO_{95} were purchased from Polymer Source Inc. (Montreal, Canada). The PAA-*b*-PAAm, $PDMAEMA_{150}$, and PAA_{51}-*b*-PEO_{250} polymers were used as received. The P2VP and P2VP-*b*-PEO polymers were quaternised with methyl iodide. Elemental analysis on four randomly chosen batches of quaternised P2VP and P2VP-*b*-PEO polymers, yielded a degree of quarternisation of 89% for all samples. Hence, we presume all batches of P2VP and P2VP-*b*-PEO polymers to be quaternised for about 89%. Polymer characteristics are summarised in table 1 (subscripts correspond to the degree of polymerisation).

Table 1. Polymer characteristics: molecular weight, $M_w/\mathrm{g\,mol^{-1}}$ and polydispersity index, PDI.

Polymer	M_w [a]	PDI [b]
PAA_{39}-*b*-$PAAm_{97}$	9977	1.21
PAA_{39}-*b*-$PAAm_{191}$	16659	1.23
PAA_{39}-*b*-$PAAm_{381}$	30164	1.22
PAA_{44}-*b*-$PAAm_{150}$	14105	1.10
PAA_{44}-*b*-$PAAm_{300}$	24767	1.17
PAA_{44}-*b*-$PAAm_{610}$	46801	1.23
$P2MVP_{41}$-*b*-PEO_{95}	13672	1.07
$P2MVP_{38}$-*b*-PEO_{211}	18088	1.01
$P2MVP_{42}$-*b*-PEO_{446}	29366	1.02
$P2MVP_{71}$-*b*-PEO_{454}	36428	1.02
PAA_{51}-*b*-PEO_{250}	14688	1.10
$P2MVP_{43}$	9950	1.10
$PDMAEMA_{150}$	23582	1.04

[a] For PAA-*b*-PAAm copolymers including the mass of the CTA, $272\,\mathrm{g\,mol^{-1}}$. For P2MVP-*b*-PEO copolymers assuming 89% quarternisation, mass including counterion iodide.
[b] For PAA-*b*-PAAm copolymers determined by gel permeation chromatography (GPC) in water.

2.2 Sample preparation

For all (*i.e.*, light and neutron scattering) experiments, polymer stock solutions were prepared by dissolution of known amounts of polymer into D_2O (> 99% isotope purity, Aldrich) to which known amounts of $NaNO_3$ (up to a concentration of 1 mM $NaNO_3$) were added, followed

by a pH adjustment using 0.1 and 1.0 M NaOD and DCl. The measured $p\mathrm{H}_{\mathrm{app}}$ value was corrected for the known shift in proton activity upon 100% substitution of hydrogen into deuterium by adding 0.408 to obtain the pD [9]. Polymer stock solutions were filtered over 0.20 μm Schleicher and Schuell filters prior to mixing. C3Ms were prepared by mixing the polymer stock solutions at the preferred micellar composition, PMC, corresponding to a 1:1 ratio of charged groups in case of strong polyelectrolytes and to a pH-dependent value of the mixing fraction, f_+ in case of weak polyelectrolytes. The mixing fraction is herein defined as the ratio between the number of positively chargeable (2VP or DMAEMA) and charged (2MVP) monomers and the sum of the numbers of positively and negatively chargeable and charged monomers (2VP, DMAEMA, 2MVP, and AA), *i.e.*,

$$f_+ = \frac{[n_+]}{[n_+] + [n_-]} \,. \tag{1}$$

Previously, it was established that polymer stock solutions prepared at a pD ~ 7 result in a PMC at $f_+ = 0.5$ for the combination PDMAEMA/PAA [10], while the stock solutions should be prepared at pH ~ 8 for the combination P2MVP/PAA [11–13]. Unless otherwise specified, all experiments were performed at room temperature.

2.3 Methods

2.3.1 Static and dynamic light scattering (SLS/DLS)

Static and dynamic light scattering measurements have been performed on an ALV light scattering instrument equipped with an 1) ALV-5000/60 × 0 digital correlator and a Lexel 85 400 mW argon ion laser (C3Ms of PAA-*b*-PAAm and $\mathrm{P2MVP}_{43}$; C3Ms of P2MVP-*b*-PEO and PAA_{51}-*b*-PEO_{250}) or an 2) ALV-5000 digital correlator and a Spectra Physics 2000 1 W argon ion laser (C3Ms of PAA-*b*-PAAm and $\mathrm{PDMAEMA}_{150}$), both operated at a wavelength, λ, of 514.5 nm. A refractive index matching bath of filtered *cis*-decalin surrounded the cylindrical scattering cell, and the temperature was controlled at 1) $25.0 \pm 0.3\,^{\circ}$C using a Haake F8-C35 thermostat and at 2) $21.9 \pm 0.1\,^{\circ}$C using a Haake F3-K thermostat. The second-order correlation function, $G_2(t)$ and total averaged scattered intensity were recorded 5 times per angle, for 24 angles, θ, from 30° to 145° in increments of 5° to evaluate the angular dependence of the diffusion coefficient, D, and the excess Rayleigh ratio, $R(\theta, C)$. DLS experiments have been analysed using the method of cumulants. The diffusion coefficient extrapolated to zero angle, D^0, has been obtained from the slope in a plot of the average frequency, Γ *versus* q^2 and has been converted into a hydrodynamic radius, R_h^0 via the Stokes-Einstein equation. SLS experiments have been analysed in terms of the Zimm (2) and Guinier approximation (3)

$$\frac{KC}{R(\theta, C)} \approx \frac{1}{M}\left(1 + \frac{1}{3}q^2 R_g^2\right), \tag{2}$$

$$\frac{KC}{R(\theta, C)} \approx \frac{1}{M}\exp\left(\frac{1}{3}q^2 R_g^2\right), \tag{3}$$

—both valid for sufficiently dilute conditions; *i.e.*, $S(q) = 1$, and small values of qR_g— with the weight concentration of scattering particles, C, the molar mass of the scattering particles, M, the radius of gyration, R_g, an optical constant, K, being

$$K = \frac{4\pi^2 n^2}{N_{\mathrm{av}}\lambda_0^4}\left(\frac{\mathrm{d}n}{\mathrm{d}c}\right)^2, \tag{4}$$

and the magnitude of the scattering wave vector, q, being

$$q = \frac{4\pi n}{\lambda_0}\sin\left(\frac{\theta}{2}\right), \tag{5}$$

with the solvent refractive index, n, the laser wavelength, λ_0 (514.5 nm), Avogadro's number, N_{av}, and the specific refractive index increment, $\mathrm{d}n/\mathrm{d}c$.

Thus, from the intercept and slope in the extrapolation of $KC/R(\theta, C)$ to zero angle ($q = 0$) at a given concentration, one obtains the apparent micellar mass, M_{micelle} and the radius of gyration extrapolated to zero angle, R_g^0. The apparent micellar aggregation number, P_{agg}, and more specifically, the number of anionic, P_{agg}^-, and cationic, P_{agg}^+ polymers per micelle can be calculated from M_{micelle}, $M_{\mathrm{building\ block}}$ (see ref. [6] for the definition of a "building block"), and f_+. Toluene was used as a reference. Table 2 presents an overview of the relevant values of $M_{\mathrm{building\ block}}$ and $\mathrm{d}n/\mathrm{d}c$.

2.3.2 Small-angle neutron scattering (SANS)

Small-angle neutron scattering experiments were performed at the Institut Max von Laue-Paul Langevin (ILL), Grenoble, France on the D22 beam line. One (8 m, C3Ms of PAA-*b*-PAAm and $\mathrm{PDMAEMA}_{150}$) and two (4 and 17.6 m, C3Ms of PAA-*b*-PAAm and $\mathrm{P2MVP}_{43}$; C3Ms of P2MVP-*b*-PEO and PAA_{51}-*b*-PEO_{250}) detector distances were chosen, such that a q-range of 0.005–0.100 Å^{-1} and 0.005–0.137 Å^{-1}, respectively, was covered, with an incident wavelength of 0.8 nm and a wavelength resolution $\Delta\lambda/\lambda$ of 10%. The samples were contained in quartz cells (Hellma, Germany) of 1 and 2 mm path length and maintained at room temperature. The data were corrected for background scattering, detector response, the spectral distribution of the incident neutron beam, and converted to an absolute scattering cross-section $I(q)/\mathrm{cm}^{-1}$ according to standard ILL procedures. The SANS scattering curves were modelled with a form factor for polydisperse homogeneous spheres (Gaussian size distribution). For two samples (see below), a hard-sphere structure factor (Percus-Yevick closure, decoupling approximation using an average particle radius) was included. Detailed data analysis procedures have been described elsewhere [6]. Table 2 presents an overview of the relevant coherent scattering length densities, ρ.

3 Results and discussion

The structure of three types of complex coacervate core micelles (C3Ms) was investigated with light and small-

Table 2. Scattering input parameters: building block (see ref. [6] for definition) molecular weights, $M_w/\mathrm{g\,mol^{-1}}$, specific refractive index increments, $\mathrm{d}n/\mathrm{d}c/\mathrm{cm^3\,g^{-1}}$, and the coherent neutron scattering length densities, $\rho/10^{10}\,\mathrm{cm^{-2}}$. Tabulated values were calculated for polyelectrolyte blocks in charged state and in the absence of counterions.

Building block	M_w	$\frac{\mathrm{d}n}{\mathrm{d}c}$ [a]	ρ [b]
PAA_{39}-*b*-$PAAm_{97}$ + 39/43 $P2MVP_{43}$	14545	0.228	2.71
PAA_{39}-*b*-$PAAm_{191}$ + 39/43 $P2MVP_{43}$	21413	0.215	3.16
PAA_{39}-*b*-$PAAm_{381}$ + 39/43 $P2MVP_{43}$	35295	0.204	3.54
PAA_{44}-*b*-$PAAm_{150}$ + 44/43 $P2MVP_{43}$	19373	0.222	2.92
PAA_{44}-*b*-$PAAm_{300}$ + 44/43 $P2MVP_{43}$	30333	0.209	3.35
PAA_{44}-*b*-$PAAm_{610}$ + 44/43 $P2MVP_{43}$	52982	0.200	3.69
PAA_{51}-*b*-PEO_{250} + 51/41 $P2MVP_{41}$-*b*-PEO_{95}	25972	0.185	1.04
PAA_{51}-*b*-PEO_{250} + 51/38 $P2VMP_{38}$-*b*-PEO_{211}	33241	0.174	0.96
PAA_{51}-*b*-PEO_{250} + 51/42 $P2VMP_{42}$-*b*-PEO_{446}	44623	0.164	0.89
PAA_{51}-*b*-PEO_{250} + 51/71 $P2VMP_{71}$-*b*-PEO_{454}	35132	0.172	0.95
PAA_{39}-*b*-$PAAm_{97}$ + 39/150 $PDMAEMA_{150}$	16067	0.209	2.52
PAA_{39}-*b*-$PAAm_{191}$ + 39/150 $PDMAEMA_{150}$	22935	0.202	2.99
PAA_{39}-*b*-$PAAm_{381}$ + 39/150 $PDMAEMA_{150}$	36817	0.197	3.42
PAA_{44}-*b*-$PAAm_{150}$ + 44/150 $PDMAEMA_{150}$	21091	0.206	2.74
PAA_{44}-*b*-$PAAm_{300}$ + 44/150 $PDMAEMA_{150}$	32051	0.199	3.21
PAA_{44}-*b*-$PAAm_{610}$ + 44/150 $PDMAEMA_{150}$	54700	0.194	3.60

[a] Calculated using the following $\mathrm{d}n/\mathrm{d}c$ values for the monomers: 0.187 (PAAm) [23], 0.136 (PEO) [23], 0.261 (PAA) [24], 0.21 (PDMAEMA) [25], 0.27 (P2MVP) [24].

[b] Calculated using the following ρ values for the monomers: 4.15 (PAAm), 0.68 (PEO), 1.81 (PAA), 1.12 (PDMAEMA), 1.33 (P2MVP) [6,26]. Full H/D exchange is taken into account.

Table 3. Summary of light and neutron scattering results: micellar mass, $M_w/\mathrm{kg\,mol^{-1}}$, aggregation number given as the number of anionic, P^-_{agg}, and cationic, P^+_{agg} polymers per micelle, radius of hydration extrapolated to zero angle, R^0_h/nm, radius of gyration (Guinier extrapolation), R_{Gu}/nm, average core radius (model fitting), $\langle R\rangle$/nm, average shell radius, R_s/nm, core polydispersity (model fitting), p_{real}, and the ratio of the radii of gyration (Guinier extrapolation) and hydration, R_{Gu}/R^0_h. The micellar masses, M_w, are averages of Guinier and Zimm extrapolations (difference between extrapolations was $\leq$ 1 and 8%, respectively). We estimate the uncertainties in M_w, P_{agg}, R_s, and p_{real} to be in the order of 10–15% and those in R^0_h, R_{Gu}, and $\langle R\rangle$ to be $\leq$ 10%.

Polymers (M_w)	SLS/DLS			SANS				
	P^-_{agg}	P^+_{agg}	R^0_h	R_{Gu}	$\langle R\rangle$	R_s	p_{real}	R_{Gu}/R^0_h
PAA_{39}-*b*-$PAAm_{97}$ + $P2MVP_{43}$ (295)	20.3	18.4	11.5	-	8.3	3.2	0.15	-
PAA_{44}-*b*-$PAAm_{150}$ + $P2MVP_{43}$ (580)	29.9	30.6	15.8	7.4	11.2	4.6	0.17	0.47
PAA_{39}-*b*-$PAAm_{191}$ + $P2MVP_{43}$ (353)	16.5	14.9	14.1	-	10.8	3.3	0.26	-
PAA_{44}-*b*-$PAAm_{300}$ + $P2MVP_{43}$ (653)	21.5	22.0	19.5	9.4	12.5	7.0	0.25	0.48
PAA_{39}-*b*-$PAAm_{381}$ + $P2MVP_{43}$ (432)	12.2	11.1	19.3	9.3	11.5	7.8	0.27	0.48
PAA_{44}-*b*-$PAAm_{610}$ + $P2MVP_{43}$ (667)	12.6	12.9	26.1	12.8	14.5	11.6	0.28	0.49
$P2VMP_{38}$-*b*-PEO_{211} + PAA_{51}-*b*-PEO_{250} (253)	7.6	10.2	13.7	8.1	11.5	2.2	0.24	0.59
$P2VMP_{42}$-*b*-PEO_{446} + PAA_{51}-*b*-PEO_{250} (250)	5.6	6.8	16.3	9.9	13.1	3.2	0.27	0.61
$P2VMP_{71}$-*b*-PEO_{454} + PAA_{51}-*b*-PEO_{250} (517)	14.7	10.6	19.8	-	-	-	-	-

angle neutron scattering experiments: 1) C3Ms consisting of two diblock copolymers, an annealed copolymer PAA_{51}-*b*-PEO_{250} and a quenched copolymer $P2MVP_x$-*b*-PEO_y (x_1, y_1: 41, 95; x_2, y_2: 38, 211; x_3, y_3: 42, 446; x_4, y_4: 71, 454), 2) C3Ms consisting of an annealed (*p*H-dependent charge density) diblock copolymer $PAA_{39/44}$-*b*-$PAAm_z$ ($z = N_{\mathrm{PAAm}}$ = 97, 150, 191, 300, 381, and 610) and a quenched (*p*H-independent charge density) homopolymer $P2MVP_{43}$, and 3) C3Ms consisting of an annealed diblock copolymer, $PAA_{39/44}$-*b*-$PAAm_z$ ($z = N_{\mathrm{PAAm}}$ = 97, 150, 191, 300, 381, and 610) and an annealed homopolymer $PDMAEMA_{150}$. In the following, C3Ms consisting of two diblock copolymers will be referred to as D-C3Ms, while C3Ms consisting of one diblock copolymer and one homopolymer will be referred to as S-C3Ms.

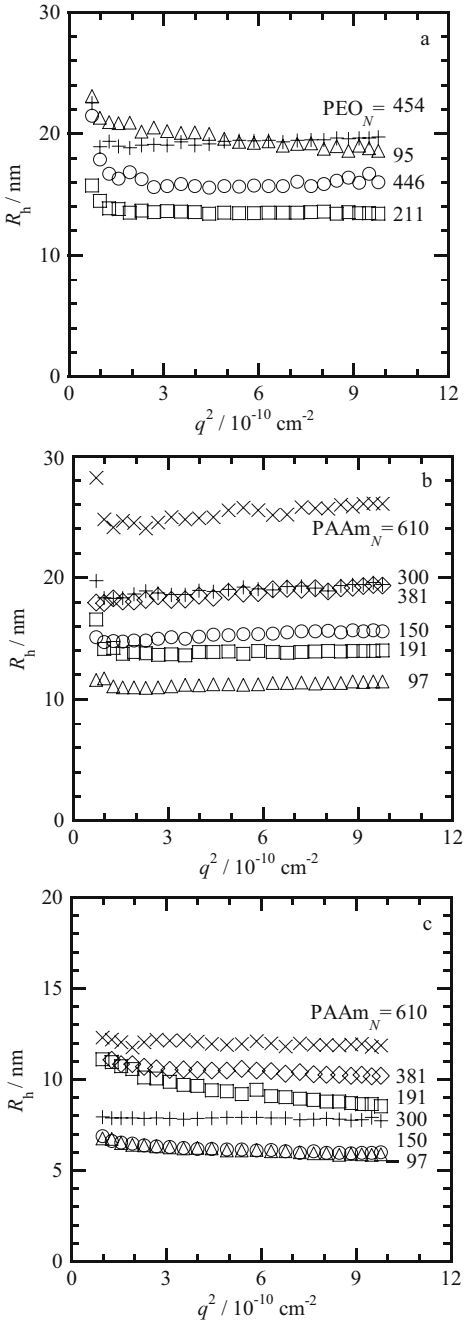

Fig. 2. DLS results (cumulant analysis). R_h^θ as a function of q^2 for aqueous solutions of C3Ms of (a) PAA$_{51}$-*b*-PEO$_{250}$ and (△) P2MVP$_{41}$-*b*-PEO$_{95}$, (□) P2MVP$_{38}$-*b*-PEO$_{211}$, (○) P2MVP$_{42}$-*b*-PEO$_{446}$, (+) P2MVP$_{71}$-*b*-PEO$_{454}$ ($f_+ = 0.50$, $C = 8.2$–$8.4\,\mathrm{g\,l^{-1}}$, $T = 25\,^\circ\mathrm{C}$), and (b) P2MVP$_{43}$ and (△) PAA$_{39}$-*b*-PAAm$_{97}$, (○) PAA$_{44}$-*b*-PAAm$_{150}$, (□) PAA$_{39}$-*b*-PAAm$_{191}$, (+) PAA$_{44}$-*b*-PAAm$_{300}$, (◇) PAA$_{39}$-*b*-PAAm$_{381}$, (×) PAA$_{44}$-*b*-PAAm$_{610}$ ($f_+ = 0.50$, $C = 8.3$–$8.6\,\mathrm{g\,l^{-1}}$, $T = 25\,^\circ\mathrm{C}$), and (c) PDMAEMA$_{150}$ and (△) PAA$_{39}$-*b*-PAAm$_{97}$, (○) PAA$_{44}$-*b*-PAAm$_{150}$, (□) PAA$_{39}$-*b*-PAAm$_{191}$, (+) PAA$_{44}$-*b*-PAAm$_{300}$, (◇) PAA$_{39}$-*b*-PAAm$_{381}$, (×) PAA$_{44}$-*b*-PAAm$_{610}$ ($f_+ = 0.50$, $C = 8.1$–$8.5\,\mathrm{g\,l^{-1}}$, $T = 25\,^\circ\mathrm{C}$). The upturns at low q-values, most pronounced for C3Ms of PAA$_{51}$-*b*-PEO$_{250}$ and P2MVP$_{41}$-*b*-PEO$_{95}$, and C3Ms of PAA$_{39}$-*b*-PAAm$_{191}$ and PDMAEMA$_{150}$, are presumably due to a small fraction of larger aggregates.

3.1 Dynamic light scattering

Figure 2 depicts the results of dynamic light scattering (DLS) measurements on D-C3Ms of PAA-*b*-PEO and P2MVP-*b*-PEO (fig. 2a), S-C3Ms of PAA-*b*-PAAm and P2MVP$_{43}$ (fig. 2b), and S-C3Ms of PAA-*b*-PAAm and PDMAEMA$_{150}$ (fig. 2c). A linear dependence of Γ on q^2 (diffusive motion) was observed for all samples, resulting in the hydrodynamic radii, R_h^0 as presented in table 3. For the sake of completeness, we provide all experimentally determined values in the electronic supporting information (table S1), while only those values that we regard as reliable enough for quantitative interpretation are listed in table 3 in the main text of this contribution. We find a nearly constant value of R_h^θ for all values of q^2, with the exception of D-C3Ms of PAA$_{51}$-*b*-PEO$_{250}$ and P2MVP$_{41}$-*b*-PEO$_{95}$ and S-C3Ms of PAA$_{39}$-*b*-PAAm$_{191}$ and PDMAEMA$_{150}$. The q-dependence of R_h^θ in these samples is probably caused by a small fraction of larger aggregates (note also the upturns at low-q values in the SLS results).

As expected, R_h^0 increases upon increasing N_{corona}. S-C3Ms co-assembled from PAA$_{44}$-*b*-PAAm and P2MVP$_{43}$ have a slightly larger R_h^0 than those co-assembled from PAA$_{39}$-*b*-PAAm and P2MVP$_{43}$, *i.e.*, for these S-C3Ms the micellar size increases with increasing N_{corona} and N_{core}. On the other hand, we find the opposite dependence of R_h^0 on N_{core} for S-C3Ms of PAA-*b*-PAAm and PDMAEMA$_{150}$. This might be related to the disparity in the polyelectrolyte block length, *i.e.*, $N_{\mathrm{PDMAEMA}} = 150$, while $N_{\mathrm{PAA}} = 39$ and 44, but currently, we are lacking a satisfactory, tentative explanation.

3.2 Static light scattering

The micellar mass, M_{micelle}, the radius of gyration extrapolated to zero angle, R_g^0, and the number of anionic, P_{agg}^-, and cationic, P_{agg}^+, polymers per micelle can be obtained from the angular dependence of the excess Rayleigh ratio, $R(\theta, C)$ (fig. 3). Averaged values of the Guinier and Zimm extrapolations are given in table 3, as the differences are small ($\leq 8\%$). In agreement with our previous findings [6], P_{agg}^- and P_{agg}^+ were found to decrease with increasing N_{corona} and in analogy to the DLS results, P_{agg}^- and P_{agg}^+ were found to increase with increasing N_{core} for S-C3Ms of PAA-*b*-PAAm and P2MVP$_{43}$. Both results can easily be rationalised with a simple geometrical model [10]. With increasing N_{corona}, the polymers strive to occupy a larger area at the core-corona interface, reducing the core radius (to increase the surface-to-volume ratio), resulting in a smaller aggregation number. Similarly, with increasing N_{core}, the core radius is increased, resulting in a larger aggregation number. Surprisingly, for S-C3Ms of PAA-*b*-PAAm and PDMAEMA$_{150}$, we find lower P_{agg}^- and P_{agg}^+ for larger N_{core}. We suppose that this system is under some kind of (so far unknown) stress, indicated by the extremely low aggregation numbers, *i.e.*, they actually correspond to the smallest physically reasonable value, as $P_{\mathrm{agg}}^+ \sim 1$. Indeed, we will exclude this system from further quantitative analysis as the aggregates are hardly to

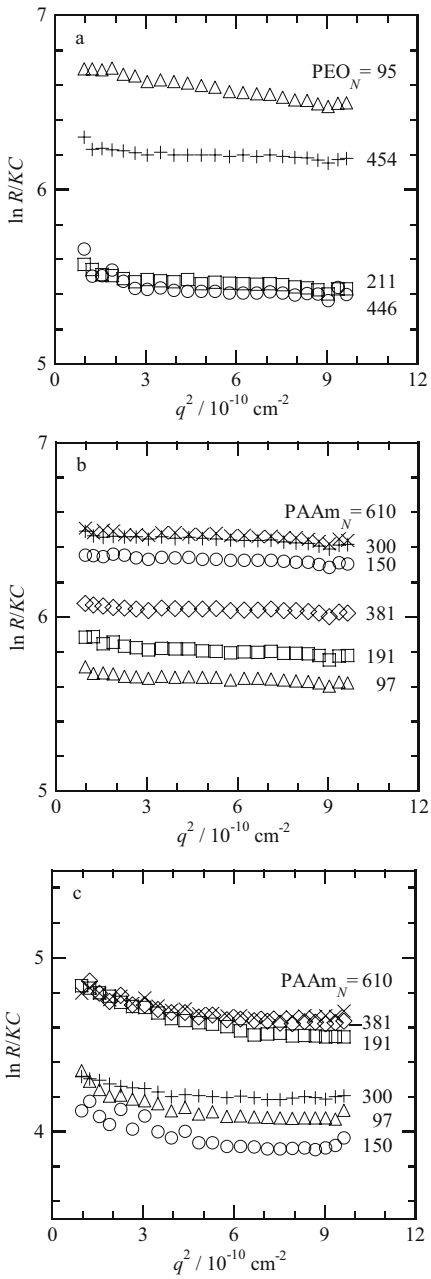

Fig. 3. Static light scattering results. Guinier representations. ln R/KC as a function of $q^2/10^{-10}\,\mathrm{cm}^{-2}$. Symbols as in fig. 2. Data points for $\theta = 30°$ (and 35° for C3Ms of PAA$_{39}$-*b*-PAAm$_{381}$ and PDMAEMA$_{150}$) have been excluded from the Zimm and Guinier analysis as they exhibit considerable upturns presumably due to a small fraction of larger aggregates. Results are listed in table 3.

be regarded as micelles. As expected, micellar mass, aggregation number, and size are a bit smaller for the S-C3Ms of PAA-*b*-PAAm and P2MVP$_{43}$ reported here, as compared to our earlier results on C3Ms of PAA$_{42}$-*b*-PAAm$_y$ and P2MVP$_{209}$ ($y = N_{\mathrm{PAAm}} = 97$, 208, and 417) [6], *i.e.*, differing only in N_{core}. Apart from low-q upturns, presumably due to a small fraction of aggregates, the q-dependence of $R(\theta, C)$ is not very pronounced, impeding an accurate determination of R_g^0. This is to be expected as, for the majority of samples, $(qR_h^0)^2$ is quite small, *i.e.*, their sizes are just within the Rayleigh limit, as $R_h^0 < \lambda/20 = 26\,\mathrm{nm}$. For the sake of completeness, R_g^0 and R_g^0/R_h^0 are given in table S1 in the electronic supporting information (typical values range from 0.6 to 1.3 as previously observed for spherical complex coacervate core micelles [6,14]). We regard them as insufficiently reliable to be included in further quantitative data analysis and they are therefore omitted from table 3.

3.3 Small-angle neutron scattering

Small-angle neutron scattering experiments were performed to study the structure and morphology of the C3Ms in more detail. As our previously reported SANS data on S-C3Ms of PAA-*b*-PAAm and P2MVP$_{209}$ could be well described with a form factor for polydisperse homogeneous spheres [6], we first attempted to apply this "bare-core approximation" to the current data set. A form factor for polydisperse homogeneous spheres applying a Gaussian size distribution was selected for this purpose. Figure 4 clearly shows that all experimental curves could be well described with such a first-order micellar model (fit results are given in table 3). Note that the $\sim 5.3\,\mathrm{g\,l^{-1}}$ solutions were sufficiently dilute to ignore interparticle interference effects, except for two samples, namely C3Ms of P2MVP$_{43}$ and PAA$_{39}$-*b*-PAAm$_{97}$ and PAA$_{39}$-*b*-PAAm$_{191}$. An additional $S(q)$ term, in the form of a hard-sphere structure factor (Percus-Yevick closure), was applied to describe the experimental data in the low-q region.

The SANS scattering curves in fully deuterated water are dominated by the scattering of the micellar core, due to very low relative polymer volume fractions in the micellar corona. Hence, $\langle R \rangle$ as obtained from model fitting provides an estimate for the core radius, R_c. Taking R_h^0 as the micellar radius, we can obtain a rough estimate for the shell radius, R_s from the difference between these two values, *i.e.*, $R_s = R_h^0 - \langle R \rangle$. Both $\langle R \rangle$ and R_s, as well as the size polydispersity, p_{real}, increase with increasing N_{corona} (table 3, fig. 5c, d). The observed increase in R_c upon increasing N_{corona} is in contradiction with all known micellization theories [15–20], and likely to result from the fact that $\langle R \rangle \neq R_c$, but in fact contains contributions from both core and corona scattering, with the latter contribution becoming increasingly important as N_{corona} increases. To verify this hypothesis unambiguously is a hard task for the present system (even if contrast-variation techniques would be applied), wherein both core and corona suffer from low contrast in microscopy and scattering experiments due to the high solvent volume fraction. It would perhaps be feasible upon replacement of the homopolymer by a stronger scatterer, such as a nanoparticle or a coordination polymer containing heavy metal ions. At present, we merely state that R_c should be regarded as an upper limit for the core radius and R_{shell} as a lower limit for the shell radius. Rather strikingly, we find $R_s < R_c$ for all systems, *i.e.*, the C3Ms of PAA-*b*-PAAm and P2MVP, and

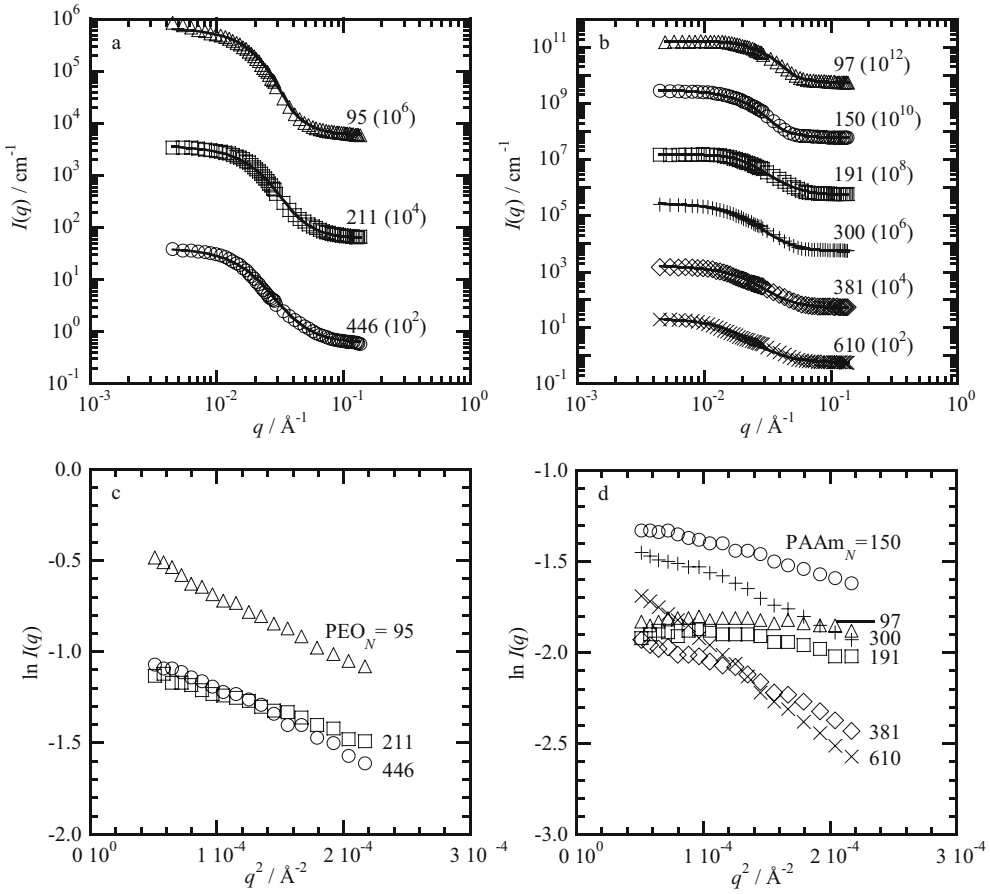

Fig. 4. SANS results. (a, b) Scattering curves, $I(q)/\mathrm{cm}^{-1}$ *versus* $q/\mathrm{Å}^{-1}$ and (c, d) Guinier representations, $\ln I(q)$ *versus* $q^2/\mathrm{Å}^{-2}$ for C3Ms of (a, c) PAA_{51}-*b*-PEO_{250} and (△) $P2MVP_{41}$-*b*-PEO_{95}, (□) $P2MVP_{38}$-*b*-PEO_{211}, (○) $P2MVP_{42}$-*b*-PEO_{446}, ($f_+ = 0.50$, $C = 5.1$–$5.3\,\mathrm{g\,l^{-1}}$, $T = 25\,°\mathrm{C}$), and (b, d) $P2MVP_{43}$ and (△) PAA_{39}-*b*-$PAAm_{97}$, (○) PAA_{44}-*b*-$PAAm_{150}$, (□) PAA_{39}-*b*-$PAAm_{191}$, (+) PAA_{44}-*b*-$PAAm_{300}$, (◇) PAA_{39}-*b*-$PAAm_{381}$, (×) PAA_{44}-*b*-$PAAm_{610}$ ($f_+ = 0.50$, $C = 5.1$–$5.3\,\mathrm{g\,l^{-1}}$, $T = 25\,°\mathrm{C}$). Fit results are listed in table 3. (a-c) Scattering curves include incoherent scattering due to solvent and hydrogenated polymer segments. Markers correspond to experimental data; solid lines represent model fitting results. The model includes a form factor for polydisperse homogeneous spheres (in combination with a hard-sphere structure factor (Percus-Yevick closure) for C3Ms of $P2MVP_{43}$ and PAA_{39}-*b*-$PAAm_{97}$/PAA_{39}-*b*-$PAAm_{191}$). The used q-range is 0.005–$0.137\,\mathrm{Å}^{-1}$. When necessary (due to lack of statistics and/or upturns resulting from a small fraction of aggregates), the first 1-3 points were discarded. N_{corona} and the off-set factor used to rescale the scattering curves for better visibility are indicated in the figure. (d-f) The used q-range is $0.007 < q < 0.15\,\mathrm{Å}^{-1}$. Data points $\leq 0.007\,\mathrm{Å}^{-1}$ were discarded due to lack of statistics and/or upturns resulting from a small fraction of aggregates. The q-range for the experiments on S-C3Ms of PAA-*b*-PAAm and $PDMAEMA_{150}$ was too limited to obtain reliable values from model fitting. All other results are given in the electronic supplementary information (fig. S1).

PAA-*b*-PEO and P2MVP-*b*-PEO are all in the so-called "crew-cut" regime (that is, $R_s < R_c$), even for very large ratios of N_{corona} to N_{core}. Tentatively, we attribute this finding to the high core solvent fraction. For all types of C3Ms studied here, the Guinier radius, R_{Gu}, was found to increase with increasing N_{corona} (fig. 5b). The resulting R_{Gu}/R_h^0 values are very low, as observed previously for C3Ms of PAA_{42}-*b*-$PAAm_{97}$ and $P2MVP_{209}$ [6].

3.4 Scaling behaviour

As mentioned in the introduction, this study was intended not only to investigate the structure and morphology of C3Ms, but furthermore, to compare the scaling behaviour of micellar aggregation numbers and radii with the theoretical predictions developed for micelles consisting of polymer amphiphiles. To do so, the scattering results described in this paper are summarised in fig. 5 and table 3. From the above discussion, it is clear that $\langle R \rangle$ cannot be unambiguously attributed to the core, and we thus refrain from including R_c and R_{shell} in the discussion of the scaling behaviour. Qualitatively, it is evident that R_h and R_{Gu} increase quasi-linearly with increasing N_{corona}, while P_{agg} decreases almost linearly upon increasing N_{corona}. These dependencies on N_{corona} are inconsistent with scaling law predictions for traditional polymeric micelles in any (*i.e.*, star-like or crew-cut) limit [16–20], as demonstrated in fig. 5c, presumably due to several generic C3M characteristics, such as the relatively high

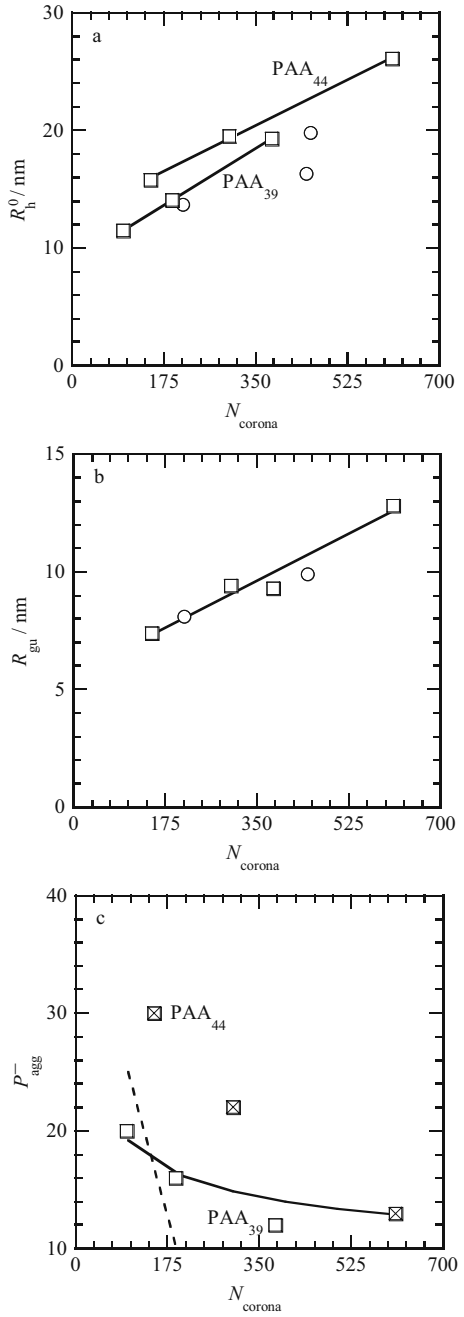

Fig. 5. (a) R_h^0, (b) R_{Gu}, and (c) P_{agg}^- as a function of N_{corona} for C3Ms of (○) $\mathrm{PAA_{51}}$-*b*-$\mathrm{PEO_{250}}$ and P2MVP-*b*-PEO, and (□) $\mathrm{P2MVP_{43}}$ and PAA-*b*-PAAm. The solid and dashed lines represent asymptotic star-like and crew-cut scaling. We estimate the uncertainties in P_{agg} to be in the order of 10–15% and those in R_h^0 and R_{Gu} to be $\leq 10\%$.

core solvent fraction, the low core-corona interfacial tension, and the high solubility of the coronal chains. This may well be the reason why a recently proposed primitive first-order self-consistent field (SCF) theory for obligatory co-assembly [21] does correctly predict the dependence of micellar size on N_{corona}. A recently developed scaling theory for the crossover regime is likewise more successful [20,22]. It is clear that a more stringent test of these theories, including a larger variation of N_{corona}, precise determination of R_c and R_{shell} as well as of several prefactors, such as stiffness parameters and the core surface tension, would provide a much better insight. For S-C3Ms of PAA-*b*-PAAm and $\mathrm{P2MVP_{43}}$, we find larger micelles (mass, size, and aggregation numbers) for $N_{\mathrm{PAA}} = 44$ as compared to $N_{\mathrm{PAA}} = 39$, and similarly, larger numbers for S-C3Ms of PAA-*b*-PAAm and $\mathrm{P2MVP_{209}}$ [6] as compared to $\mathrm{P2MVP_{43}}$. As expected, the effect of N_{core} on P_{agg} is much more pronounced than the effect of N_{corona}: a $\sim 10\%$ increase in N_{core} (from 39 to 44) results in a nearly two-fold P_{agg}, while a two-fold decrease in N_{corona} is still insufficient to achieve the same increase in P_{agg}.

4 Summary and conclusions

Light scattering and small-angle neutron scattering experiments were performed on spherical C3Ms of PAA-*b*-PEO and P2MVP-*b*-PEO, PAA-*b*-PAAm and P2MVP, and PAA-*b*-PAAm and $\mathrm{PDMAEMA_{150}}$. C3Ms of PAA-*b*-PEO and P2MVP-*b*-PEO, and C3Ms of PAA-*b*-PAAm and P2MVP were all found to be of the "crew-cut" type, *i.e.*, the core radius, R_c, is larger than the shell radius, R_s, even for very large ratios of N_{corona} to N_{core}. The dependencies of micellar size and aggregation number on N_{corona} were inconsistent with scaling laws developed for traditional polymeric micelles in the star-like and crew-cut limit. We attribute these findings to several generic C3M characteristics, such as the relatively high core solvent fraction, the low core-corona interfacial tension, and the high solubility of the coronal chains. A recently proposed primitive first-order self-consistent field theory for obligatory co-assembly does correctly predict the dependence of micellar size on N_{corona} [21], indicating that the tested scaling relationships may become applicable to C3Ms, once solvent penetration into the micellar core and a low core-corona interfacial tension are correctly taken into account. A recently developed theory for the crossover regime, *i.e.*, between the star-like and crew-cut limit, seems a very promising candidate. Future work should include 1) a set of copolymers with a larger variation in N_{corona} wherein the corona blocks are all polymerized from an identical precursor and 2) in-depth scattering studies including contrast variation techniques on suitable model systems such that more characteristics, such as R_c and R_{shell} may be determined in a reliable fashion.

This work is part of the research programme of the Stichting voor Fundamenteel Onderzoek der Materie (FOM), which is financially supported by the Nederlandse Organisatie voor Wetenschappelijk Onderzoek (NWO). It has been carried out in the framework of the EU Polyamphi/Marie Curie program (FP6-2002, proposal 505027). One of us was financed by the SONS Eurocores program (Project JA016-SONS-AMPHI). We thank ILL for providing the beam time. We thank A. Müller and P. Millard for the synthesis of the PAA-*b*-PAAm copolymers. H. Schmalz is gratefully acknowledged for the synthesis of the P2MVP-*b*-PEO copolymers. We thank F. A. M. Leermakers and T. Hellweg for fruitful discussions.

References

1. H.G. Bungenberg de Jong, H.R. Kruyt, Proc. Koninkl. Akad. Wetensch. **32**, 849 (1929).
2. A.V. Kabanov *et al.*, Macromolecules **29**, 6797 (1996).
3. A. Harada, K. Kataoka, Macromolecules **28**, 5294 (1995).
4. M.A. Cohen Stuart, N.A.M. Besseling, R.G. Fokkink, Langmuir **14**, 6846 (1998).
5. J.F. Gohy, S.K. Varshney, R. Jerome, Macromolecules **34**, 3361 (2001).
6. I.K. Voets *et al.*, Macromolecules **40**, 8476 (2007).
7. S. van der Burgh, A. de Keizer, M.A. Cohen Stuart, Langmuir **20**, 1073 (2004).
8. P.E. Millard *et al.*, in preparation (2009).
9. P. Salomaa, L.L. Schaleger, F.A. Long, J. Am. Chem. Soc. **86**, 1 (1964).
10. B. Hofs *et al.*, Phys. Chem. Chem. Phys. **8**, 4242 (2006).
11. I.K. Voets *et al.*, Angew. Chem. Int. Ed. **45**, 6673 (2006).
12. I.K. Voets *et al.*, Soft Matter **5**, 999 (2009).
13. I.K. Voets *et al.*, Langmuir **24**, 12221 (2008).
14. I.K. Voets, A. de Keizer, M.A. Cohen Stuart, Adv. Colloid Interface Sci. **147-148**, 300 (2009).
15. E.Y. Kramarenko, A.R. Khokhlov, P. Reineker, J. Chem. Phys. **125**, 194902 (2006).
16. A. Halperin, Macromolecules **20**, 2943 (1987).
17. J. Noolandi, K.M. Hong, Macromolecules **16**, 1443 (1983).
18. R. Nagarajan, K. Ganesh, J. Chem. Phys. **90**, 5843 (1989).
19. N. Dan, M. Tirrell, Macromolecules **26**, 4310 (1993).
20. E.B. Zhulina *et al.*, Macromolecules **38**, 5330 (2005).
21. I.K. Voets, F.A.M. Leermakers, Phys. Rev. E **78**, 061801 (2008).
22. I. Larue *et al.*, Macromolecules **41**, 6555 (2008).
23. P. Molyneux, *Water-Soluble Synthetic Polymers: Properties and Behavior* (CRC Press, 1982).
24. J. Brandrup, E.H. Immergut (Editors), *Polymer Handbook*, 3rd edition (John Wiley & Sons, 1989).
25. N.G. Hoogeveen, M.A. Cohen Stuart, G.J. Fleer, J. Colloid Interface Sci. **182**, 133 (1996).
26. A.S. Lee *et al.*, Macromolecules **32**, 4302 (1999).